PROCEEDINGS, 46th Workshop on Geothermal Reservoir Engineering
Stanford University, Stanford, California, February 15-17, 2021
SGP-TR-218

A Numerical Study for Determining Lateral Thermal Gradient Based on Reservoir Properties

Aburiza Akhmad, Budiman Putra, Mutiara Sihombing, Salsabila Tantri Ayu, Theresia Yolanda

AILIMA, Jakarta, Indonesia.

aburizaakhmad@ailima.co.id, budimanputra@ailima.co.id, mutiara@ailima.co.id, salsabila@ailima.co.id, theresia.yolanda@ailima.co.id

Keywords: Numerical study, lateral thermal gradient, permeability, up-flow temperature.

ABSTRACT

Unlike other renewable energy, geothermal resources are located beneath the surface. As a result, geothermal subsurface interpretation has been known to possess uncertainties. Uncertainties in thermal gradient calculation can lead to large errors in the predicted top of reservoir depth, thus unduly influencing geothermal resource estimation's precision and accuracy. It may impact the drilling cost, production performance, and the well lifetime. The geothermal thermal gradient wells require numerical models rather than conventional analytical models due to high uncertainties of temperatures and reservoir complexity, especially in permeability distribution.

This paper examines the permeability and up-flow temperature sensitivity analysis to reduce thermal gradient uncertainties. Two different permeability models have been studied: fault-hosted and distributed fracture network permeabilities. A further result of lateral thermal gradient is simulated using PetraSim. The numerical model result indicates that the distributed fracture model's thermal gradient range values are 4.08-10.87°C / km for liquid layer and 0.46-0.53°C / km for two-phase layer. While for the fault-hosted models, the thermal gradient range values are 3.16-24.93°C / km for liquid layer and 0.74-2.19°C / km for two-phase layer.

1. INTRODUCTION

Thermal gradient has an average value of 1°C/km, measured between the earth's center of the earth and atmosphere's outer limits (Lowrie, 1997) and caused by subsurface heat dissipation. Thermal gradient varies within different places due to rock conditions, regional and local heat sources (Wenas, 2020). Geothermal gradient is a reliable indicator of temperature distribution and is becoming one of the most frequently used variables for geophysical logging. (Kutasov and Eppelbaum, 2009). It is also useful in assessing an area's geothermal resource potentials (Nwankwo and Ekine, 2009) and must be addressed with other principal resource risks, such as the depth of the resource, output, and flow sustainability producing wells. Understanding thermal gradient both vertically and laterally is vital in the development of a conceptual field model.

The presented studies will provide insight into understanding the lateral thermal gradient of two different types of geothermal reservoir permeability models. It determines the lateral thermal gradient range for both network permeability and fault-hosted systems. The general workflow is applicable for other geothermal sites consisting of similar constraints.

This study's objectives are as follows:

a) To construct numerical reservoir models for distributed fracture system and fault-hosted permeability system.
b) To calculate lateral thermal gradient range for fault-hosted and distributed fracture system from sensitivity analysis of reservoir permeability and up-flow temperature.

2. LITERATURE REVIEW

Geothermal gradient is temperature measurement. It is expressed with the increase per depth happening in the Earth, which occurs because of the center's outflow conduction transportation through the crustal rocks. Geothermal gradient is averaged around 30°C/km and varies with different places. Conductive gradients around 60°C/km are measured in the crust (Grant, 2011). Lateral thermal gradients are influenced by mechanisms and geological factors, including temporal changes in thermal gradients, lithological conditions, heat flow variations, unconformities, sedimentary sequence, fluid migration in the sub-surface, and overpressures.

All geothermal systems require some permeability range to create heat convection and transport heat from below the Earth to the surface. According to Hochstein (1998), to radiate convection, a high permeability (10 mD) is needed. In low permeability layers (1 mD), there is only minor or even no convection. Permeability is one of the most important hydrologic parameters. It controls the fluid percolation in fractured and porous rock. In geothermal systems, permeability is usually controlled by the connectivity of fracture within the rock mass. Geothermal system permeability occurs because of rock masses' overburden pressure (Manning and Ingebritsen, 1999), and high permeability fault-hosted formation (Faulds et al., 2010; Taillefer et al., 2018). Geothermal resource generation depends on its geometry, field condition, permeability structure, and thermal regime (Duwiquet et al., 2019).

Understanding permeability and temperature distribution in geothermal reservoirs are fundamental, starting from exploration until field operation since geothermal subsurface interpretation has been known to possess uncertainties. Structural geological analysis can help to interpret geophysical data and identify the best case for drilling (Cacace, 2013). One of the crucial factors during geothermal exploration drilling is Top of Reservoir (T.o.R) data. It may impact the drilling cost, production performance, and the lifetime of the well.

3. METHODOLOGY

3.1 Process Flow

The process chart for this study is shown in **Figure 1**. The reservoir modelling process is carried out using PetraSim and the TOUGH2 simulator with the EOS1 single phase model. In this study, two types of reservoir models are simulated (distributed fracture and fault-hosted cases) by performing the sensitivity of permeability and up-flow temperature. Properties of rocks, fluids, wells, and heat source data are inputted to obtain the natural state simulation results. The simulation outputs, grid coordinates, and block temperature are filtered using Microsoft Excel to obtain the reservoir's first layer (top of the reservoir) data. The lateral thermal gradient cut-off process will be carried out in the area around the up-flow zone by assuming isothermal temperature in the area. The distribution calculation process is done to see the distribution and range of temperature gradients.

3.2 Limitation and Boundary

In making the numerical model, the reservoir boundary has homogeneous permeability and porosity (there is no anisotropy). In real-life cases, most geoengineering reservoirs' permeability, including geothermal reservoirs, in all three principal directions is commonly anisotropic (Snow, 1969). According to Gan and Elsworth (2014), the anisotropy shown from fracture spacing will affect heat loss with smaller fracture spacing, leading to a more extensive thermal drawdown and thermal energy recovery. A single porosity model is used for simplification in the reservoir construction process. The model is built in a natural state model, in which dual-porosity and single porosity models should give similar results. Nevertheless, suppose it is for production history where local boiling near the feed zones for some wells causes them to produce excess enthalpy fluid (O'Sullivan, 2016).

4. CASE STUDY

The model has dimensions of 10000m x 10000m with a coarsest area of 1000 m x 1000 m (representing the boundary zone), and the finest area has dimensions of 100 m x 100 m (representing the reservoir zone). The model can be seen in **Figure 2**. This model's reservoir zone has 4000 m x 4000 m for the distributed fracture model and 400 m x 4000 m for a fault-hosted model. The model is divided into eight layers with a total thickness of 2520 m. The top boundary layer (atmosphere layer) has a thickness of 20 m, 500 m for the caprock, 1500 m for the productive zone, and 500 m for the basement rock. The total number of grids is 23276. The rock properties of each layer for both cases can be seen in **Table 1**. The fluid model used is EOS1 (single-phase fluid, water). Each case's permeability will be adjusted using the correlation constructed using the first layer and basement permeability **(Figure 3)**. The permeability value of each layer for the entire case is provided in **Appendix A**. The assumptions used for this model include:

1. The heat source representing deep heat recharges into the geothermal reservoir system has a constant injection rate of 40 kg/s, with an enthalpy of 1300 kJ/kg for initial conditions.
2. The atmosphere layer uses a volume factor of 1E + 20 with an initial condition of 1 bar and 23°C to represent rocks that cannot be affected by reservoir conditions (Firdaus, 2016).
3. The heat sink at the top of the reservoir layer has a PI (productivity index) value of 1E-07 m^3 and initial pressure of 65 bar.

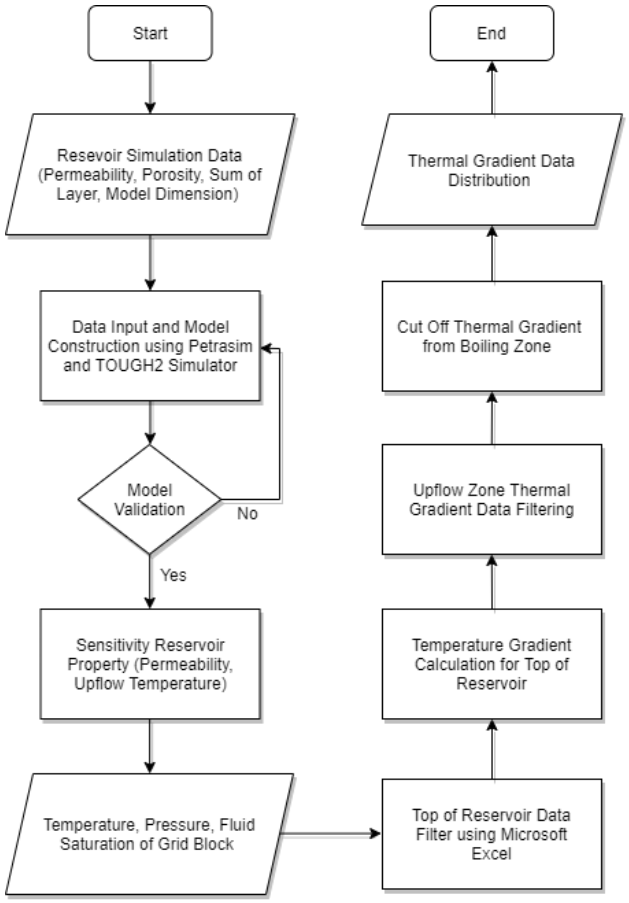

Figure 1: Workflow of this study

The simulation is done with a time limit of 1E + 05 years until the natural state conditions are reached. Sensitivity analysis is carried out by controlling the permeability value and temperature, which can be seen from the enthalpy value of the up-flow zone. The permeability used for sensitivity is 50-800 mD, while the enthalpy is ranged from 1500-1100 kJ/kg (at liquid saturation temperature 326°C-253°C). The temperature output value from each simulation is filtered with Microsoft Excel to obtain the top of reservoir zone data to then calculate the lateral thermal gradient with reference to the up-flow zone grid.

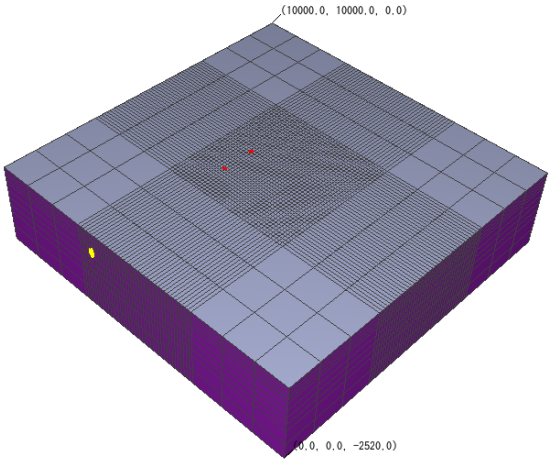

Figure 2: Reservoir 3D model

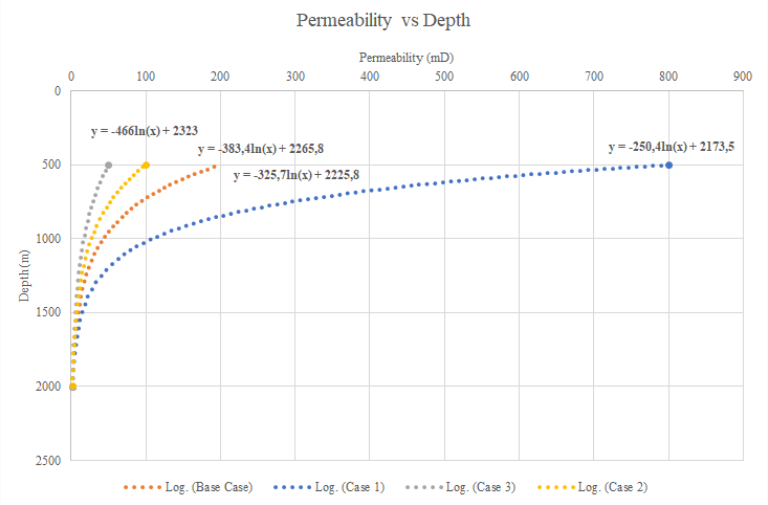

Figure 3: Permeability-Depth Correlation

Table 1: Material Properties

Material	Color	kxy (mD)	kz (mD)
ATM		1.01E-05	1.01E-05
CPR		1.01E-03	1.01E-03
RES1		200	100
RES2		140.5	70.25
RES3		60.98	30.49
RES4		26.46	13.23
RES5		11.49	5.74
BASE		2.16	5
UPL		5	40
BOND		0.010132	0.010132

5. RESULT AND DISCUSSION

The natural state model for all cases can be seen in **Figure 4** to **Figure 5**. The temperature map for all cases can be seen in **Appendix B** and **Appendix C.** It can be concluded that from the cross-section, a boiling zone is formed at the top of the reservoir layer after the steady-state condition is reached because saturation conditions have been achieved (assumed isothermal and characterized by counter- or co-current two-phase flow), which is common in the geothermal system with reservoir temperatures in the range of 300°C (Steingrímsson, 2013).

For distributed fracture, any change in permeability will affect the proportion of the boiling zone in the top layer of the reservoir, with an average increase of 30% for each decrease in permeability by half the initial conditions. According to Pruess (1983), a decrease in permeability matrix can increase flowing enthalpy and fluid mobility in the system, affecting reservoir performance and lifetime. Whereas in the fault model, there is an anomaly of decreasing fraction of boiling zone along with decreasing permeability value. This happens because using the same recharge conditions as the distributed fracture model but with a smaller productive zone size will cause an imbalance in the recharge and heat sink. From enthalpy value sensitivity, it can be obtained that the increase in enthalpy will cause the water fraction to change into 2 phases to be greater for the same top of reservoir pressure conditions (65 bar) from the phase envelope of the water phase (see **Figure 6**).

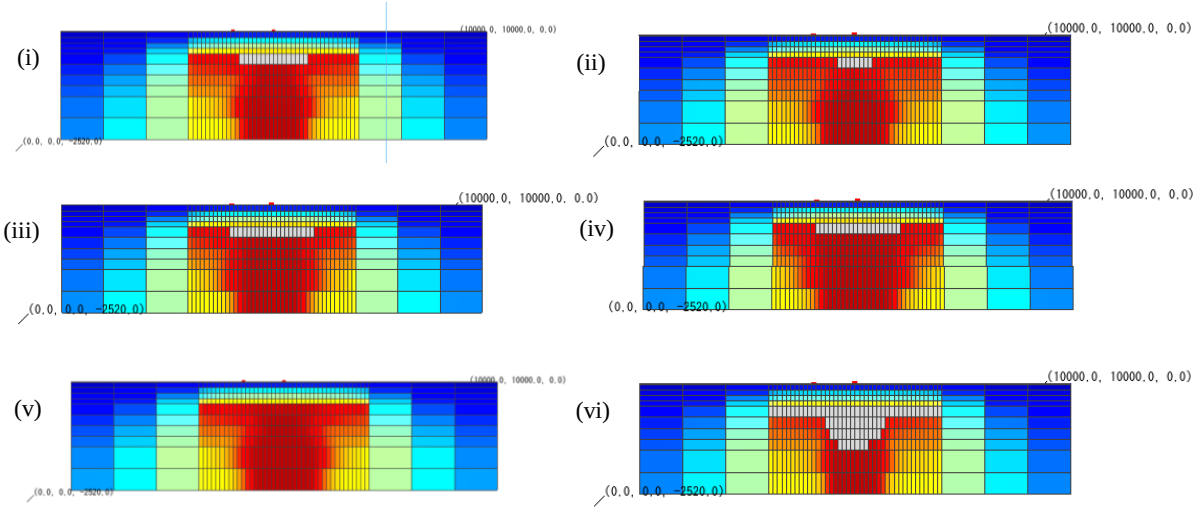

Figure 4: Model cross section distributed fracture for (i) Base Case, (ii) 800mD, (iii) 100mD, (iv) 50mD, (v) 1100kJ/kg, (vi) 1500kJ/kg

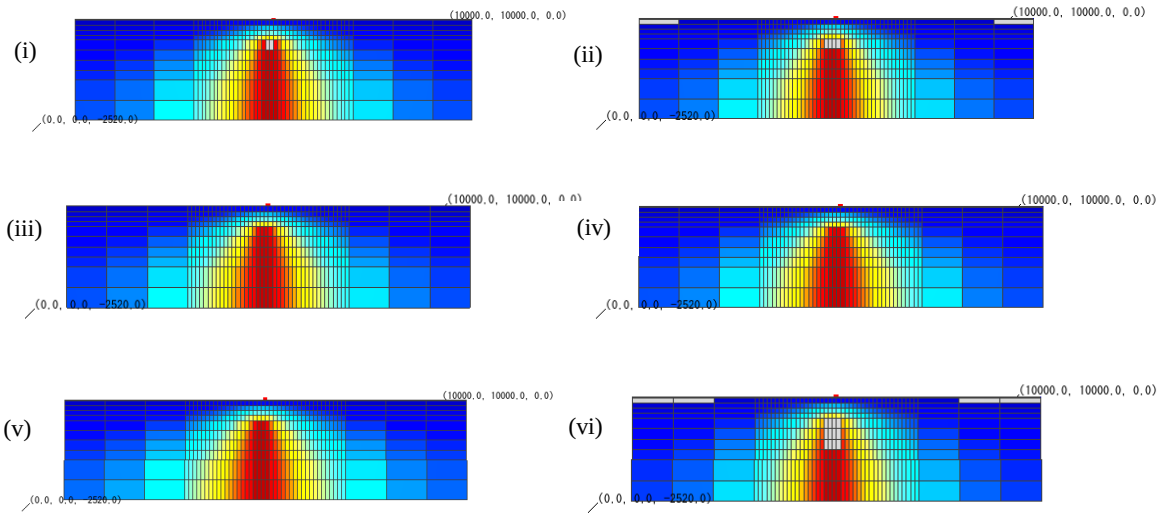

Figure 5: Model cross section fault system for (i) Base Case, (ii) 800mD, (iii) 100mD, (iv) 50mD, (v) 1100kJ/kg, (vi) 1500kJ/kg

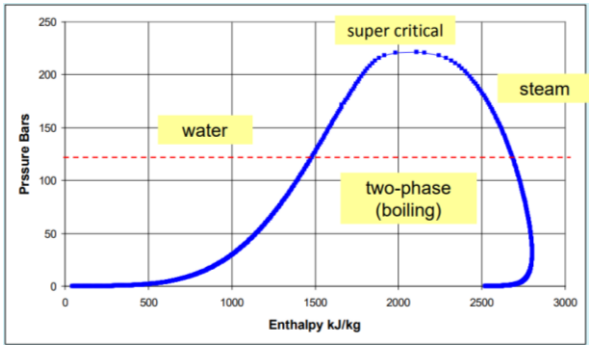

Figure 6: Water Phase Envelope

The lateral thermal gradient map for each case can be seen in **Appendix D** to **Appendix E**, and calculated using formula below

$$Lateral\ Thermal\ Gradient\ = \frac{\triangle T\ (in\ oC)}{\sqrt{\triangle i^2 + \triangle j^2}\ (in\ km)} \quad (1)$$

Where $\triangle T, \triangle i^2, \triangle j^2$ are grid block temperature, distance in i and j direction respectively,

A thermal gradient radius of the cut-off is used as a data filter before constructing a distribution curve by excluding the radius's thermal gradient data. The cut-off process is carried out when the top layer of the reservoir has a boiling zone, which is influenced by the heat source's up-flow process, and it is in the isothermal condition, which results in a very small gradient. The cut-off radius for each case can be seen in **Table 2.** The distribution curve after cut-off can be seen in **Figure 7** to **Figure 8.**

Table 2: Thermal Gradient Cut-Off Value

Distributed Fracture		
Case Name	**Cut-Off Value (°C/km)**	**Cut-Off Radius (m)**
Base Case (200mD)	0.89	900
Case 1 (800mD)	0.59	500
Case 2 (100mD)	1.1	1100
Case 3 (50mD)	1.2	1500
Case 4 (1100kJ/kg)	0.94	600
Case 5 (1500kJ/kg)	Whole Layer in 2 Phase Zone	
Fault Hosted		
Case Name	**Cut-Off Value (°C/km)**	**Cut-Off Radius (m)**
Base Case (200mD)	1.6	1100
Case 1 (800mD)	0.82	1000
Case 2 (100mD)	2	1050
Case 3 (50mD)	2	1500
Case 4 (1100kJ/kg)	Whole Layer in Compressible Liquid (No Cut-off)	
Case 5 (1500kJ/kg)	1	900

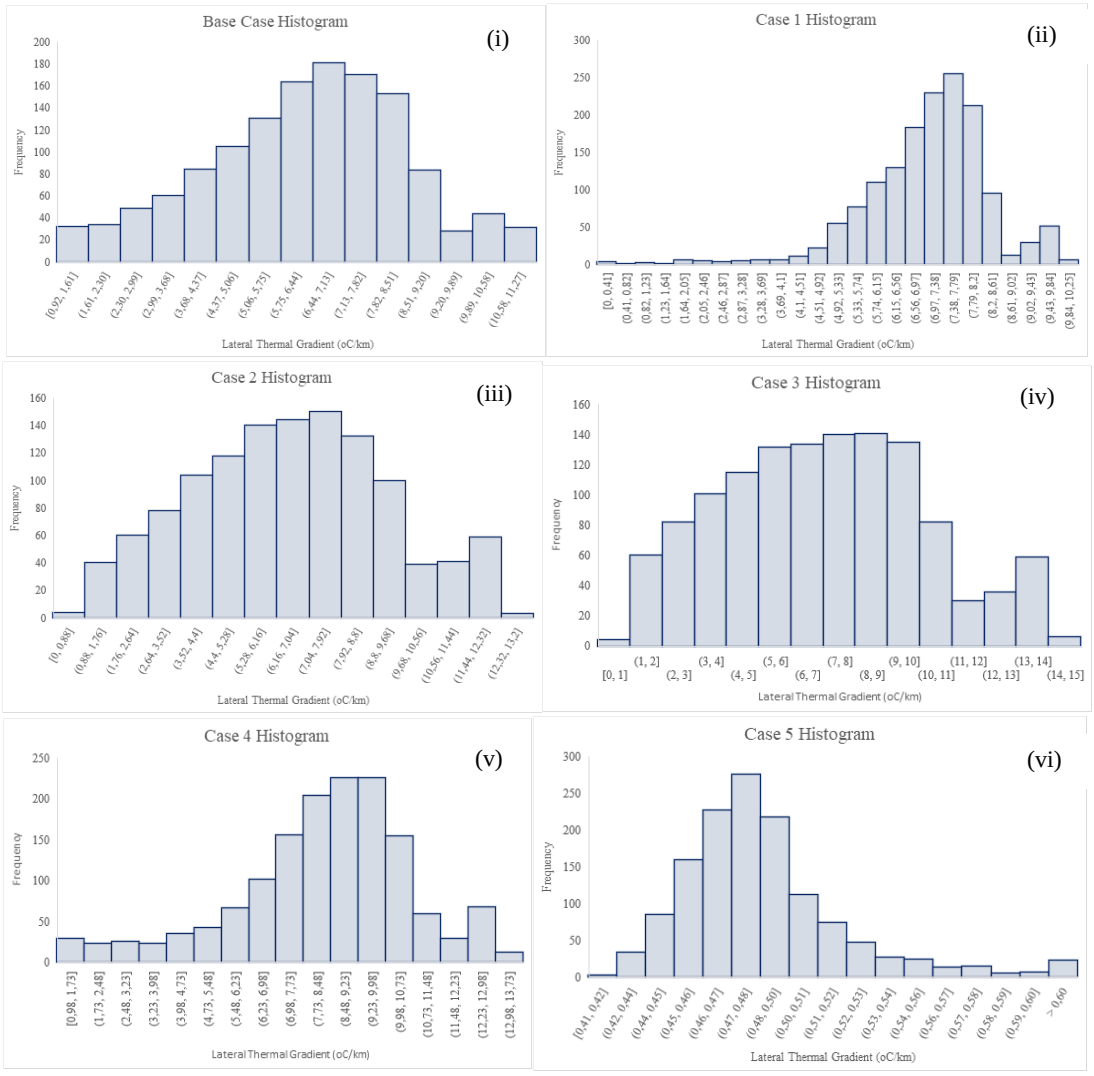

Figure 7: Lateral Thermal Gradient Histogram (Distributed Fracture) (i) Base Case, (ii) 800mD, (iii) 100mD, (iv) 50mD, (v) 1100kJ/kg, (vi) 1500kJ/kg

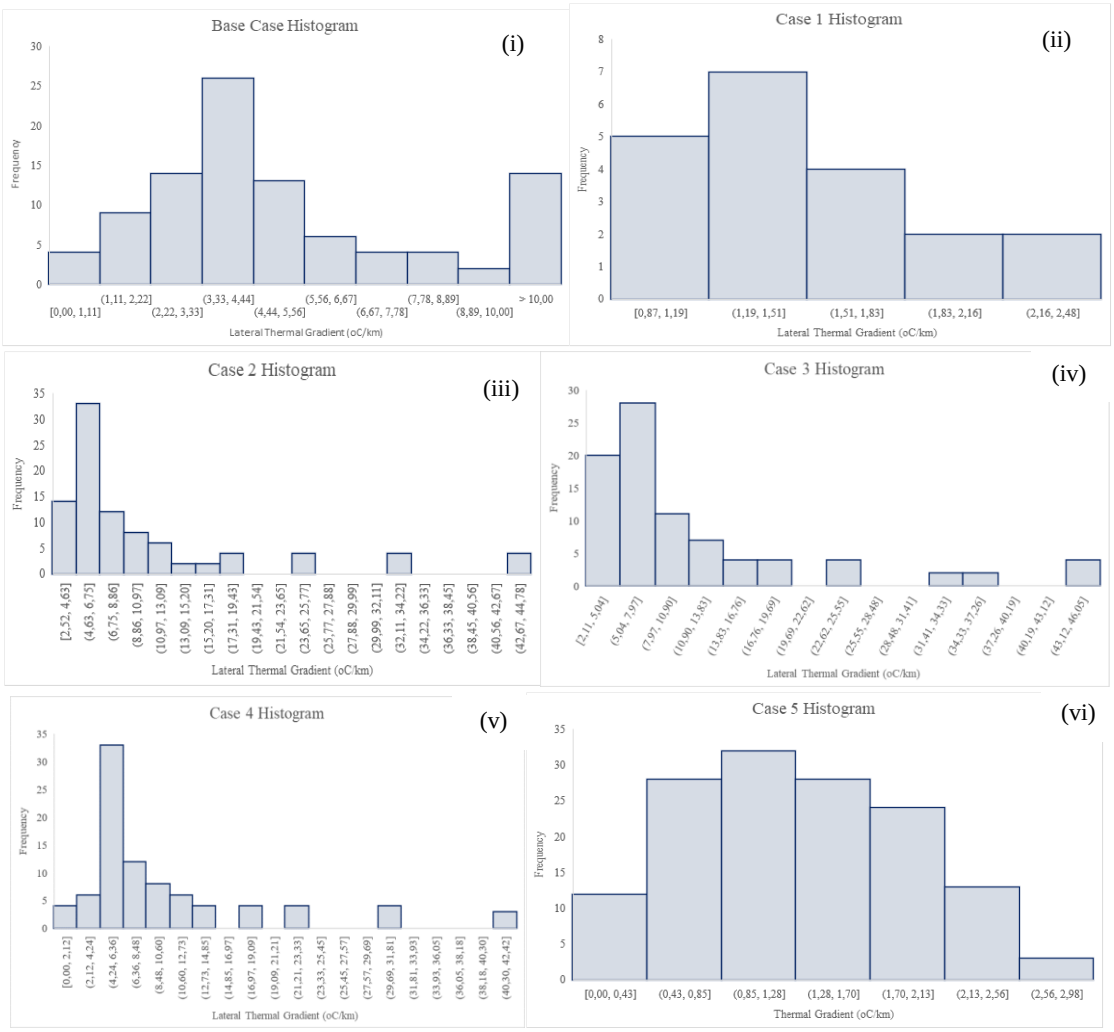

Figure 8: Lateral Thermal Gradient Histogram (Fault Hosted) (i) Base Case, (ii) 800mD, (iii) 100mD, (iv) 50mD, (v) 1100kJ/kg, (vi) 1500kJ/kg

Lateral thermal gradient range determined by using P20 and P90 data from cumulative distribution from histogram. The two models' value distribution will be divided into two types according to the type of fluid dominance seen from the thermal gradient's value and the temperature map in **Appendix B** and **Appendix C**. The thermal gradient range for the two-phase layer (mostly or filled with the boiling zone, colored in gray) is relatively small, ranging 0.46-0.53°C / km for the distributed fracture model and 0.74-2.19°C / km for the fault-hosted model. The thermal gradient results will be too small due to the isothermal effect of the area, triggered by an increase in fluid enthalpy and a decrease in pressure to the surface. For the liquid-dominated (compressed liquid) layer, the gradient range value is more significant, namely 4.08-10.87°C / km for the distributed fracture model and 3.16-24.93°C / km for the fault-hosted model. The results of the temperature gradient for both models can be seen in **Table 3.**

Table 3: Lateral Thermal Gradient Distribution

Distributed Fracture		
Case Name	**P20 (°C/km)**	**P90 (°C/km)**
Base Case (200mD)	4.45	8.92
Case 1 (800mD)	6.13	8.31
Case 2 (100mD)	4.08	10.05

Distributed Fracture		
Case Name	**P20 (°C/km)**	**P90 (°C/km)**
Case 3 (50mD)	6.48	8.95
Case 4 (1100kJ/kg)	6.63	10.87
Case 5 (1500kJ/kg)	0.46	0.53
Fault Hosted		
Case Name	**P20 (°C/km)**	**P90 (°C/km)**
Base Case (200mD)	3.16	12.97
Case 1 (800mD)	1.84	2.1
Case 2 (100mD)	4.76	24.1
Case 3 (50mD)	4.95	24.93
Case 4 (1100kJ/kg)	4.35	24.9
Case 5 (1500kJ/kg)	0.74	2.19

6. CONCLUSION

To answer the objectives, several conclusions can be drawn, namely:

1. The numerical models for distributed fracture and fault-hosted permeability reservoir can be seen in **Appendix A** and **Appendix B**. Both models have the same rock properties and initial conditions but indicate different temperature profiles and the process of forming a two-phase layer.
2. By controlling the permeability and up-flow temperature, the lateral thermal gradient values are obtained for the two models using the first productive layer (top of the reservoir). For the distributed fracture model, the thermal gradient range values are **4.08-10.87°C / km** for liquid layer and **0.46-0.53°C / km** for two-phase layer. While for the fault-hosted models, the thermal gradient range values are **3.16-24.93°C / km** for liquid layer and **0.74-2.19°C / km** for two-phase layer. The two-phase zone formation occurs at a different scale for the two models, with the fault-hosted permeability model having a larger proportion of the two-phase zone than the distributed fracture model.

7. RECOMMENDATION

This study determines the range of thermal gradients as a reference for studying the top of the reservoir using synthetic data. As a future recommendation, the limits and sensitivity variables can be simulated using field data for a better result. It is also necessary to calculate the thermal gradient's value by analyzing depth to increase accuracy so that the top of the reservoir risk determination can be reduced.

ACKNOWLEDGEMENT

This proceeding is made with support and supervision of PT Anugerah Indonesia Lima (AILIMA).

REFERENCES

Cacace M, Blocher G, Watanabe N, Moeck I, Borsing N, Kolditz O, et al.: Modelling of Fractured Carbonate Reservoirs: Outline of A Novel Technique via A Case Study from The Molasse Basin, Southern Bavaria (Germany), *Environ Earth Sci Epub*, **21**, (2013), 18.

Cant, J. L., Siratovich, P. A., Cole, J. W., Villeneuve, M. C. & Kennedy, B. M.: Matrix Permeability of Reservoir Rocks, Ngatamariki Geothermal Field, Taupo Volcanic Zone, New Zealand, *Geotherm. Energy*, **6**, (2018).

Duwiquet, H., Arbaret, L., Guillou–Frottier, L., Heap, M. J. & Bellanger, M.: On the Geothermal Potential of Crustal Fault Zones: A Case Study From The Pontgibaud Area (French Massif Central, France), *Geotherm. Energy*, **7**, (2019).

Faulds J, Coolbaugh M, Bouchot V, Moek I, Oguz K.: Characterizing Structural Controls of Geothermal Reservoirs in the Great Basin, USA, and Western Turkey: Developing successful exploration strategies in extended terranes. *Proceedings*, World Geothermal Congress Bali, Indonesia, (2010).

Firdaus, F., Sutopo & Pratama, H. B.: The Natural State Numerical Model of Patuha Geothermal Reservoir, *4th Indones. Int. Geotherm. Conv. Exhib. 2016 Proc*, Indonesia (2016), 1–13.

Gan, Q., Elsworth, D.: A Continuum Model for Coupled Stress and Fluid Flow in Discrete Fracture Networks, *Geomech. Geophys. Geo–energ. Geo–resour*, **2**, (2016), 43–61.

Hochstein MP.: Assessment and Modelling of Geothermal Reservoirs (Small Utilization Schemes), *Geothermics*, **17**, (1988), 15–49.

Ildrem, S. & Agus, N. A.: Fracture Permeability Assessment by Integration of Fracture Characterization and In Situ State of Stress in Geothermal Field, Case Study of Wayang Windu Field, (2015), 117–125.

Kutasov I M: Applied Geothermics for Petroleum Engineers, *Elsevier*, (1999).

Kutasov, I. M. & Eppelbaum, L. V.: Estimation of Geothermal Gradients from Single Temperature Log–Field Cases, *J. Geophys. Eng.* **6**, (2009), 131–135.

Lowrie W.: Fundamentals of Geophysics, *Cambridge University Press*, UK, (1997).

Malcolm A. Grant, Paul F. Bixley.: Geothermal Reservoir Engineering, *Academic Press*, (2011), 201–217.

Manning C-E, Ingebritsen S-E.: Permeability of the Continental Crust: Implications of Geothermal Data and Metamorphic Systems. *Rev Geophys*, **37(1)**, (1999), 127–50.

Nwankwo, C.N. and Ekine, A.S.: Geothermal Gradient in the Chad Basin, Nigeria, from Bottom Hole Temperature Logs. *International Journal of Physical Sciences*, **4**, (2009), 777–783.

O'Sullivan, M. J. & O'Sullivan, J. P.: Reservoir Modeling and Simulation for Geothermal Resource Characterization and Evaluation. Geothermal Power Generation: Developments and Innovation, *Elsevier Ltd*, (2016).

Pruess, K.: Heat Transfer in Fractured Geothermal Reservoirs with Boiling, *Water Resour. Res.* **19**, (1983), 201–208.

Snow DT.: Rock Fracture Spacings, Openings, and Porosities, *J Soil Mech Found Div*, **94**(1), (1968), 73–92.

Steingrimsson, B.: Geothermal Well Logging: Temperature and Pressure Logs, *Geotherm. Train. Program*, **3**, (2013), 11.

Wenas, D. R., Tulandi, D. A. & Bujung, C. A. N. Geothermal Gradient and Subsurface Temperature for Estimation of Sources, Patterns and Heat Flow Directions in the Hydrothermal Area of Minahasa Indonesia, *J. Crit. Rev.* **7**, (2020), 905–907.

,

APPENDIX

Appendix A

Permeability data for each case

Material	Depth (m)	Base Case		Case 1		Case 2		Case 3		Case 4	
		kxy (mD)	kz (mD)	kxy (mD)	kz (mD)	kxy (mD)	kz (mD)	kxy (mD)	kz (mD)	kxy (mD)	kz (mD)
RES1	500	200	100	800	400	100	50	800	400	50	25
RES2	750	140,5	70,25	294,39	147,19	52,12	26,06	294,39	147,19	29,24	14,62
RES3	1000	60,98	30,49	108,47	54,24	27,15	13,58	108,47	54,24	17,1	8,55
RES4	1250	26,46	13,23	39,97	19,98	14,15	7,07	39,97	19,98	10	5
RES5	1500	11,49	5,74	14,73	7,36	7,37	3,68	14,73	7,36	5,85	2,92

Appendix B

Temperature map for distributed fracture model (i) Base Case, (ii) 800mD, (iii) 100mD, (iv) 50mD, (v) 1100kJ/kg, (vi) 1500kJ/kg

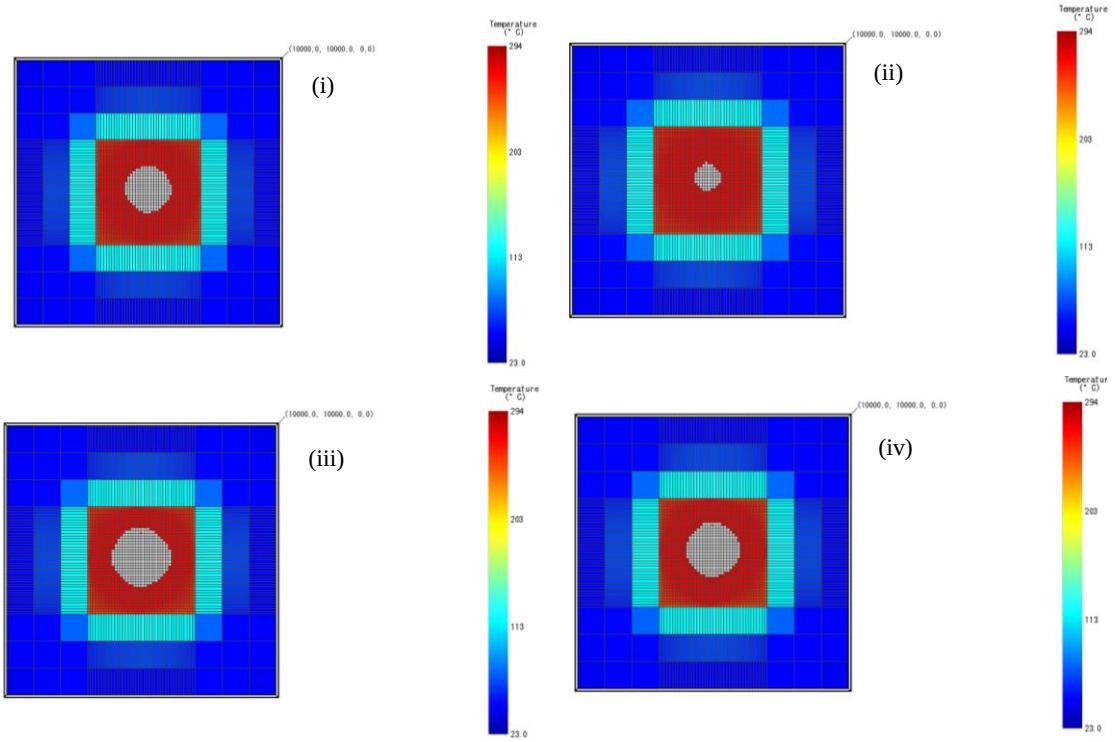

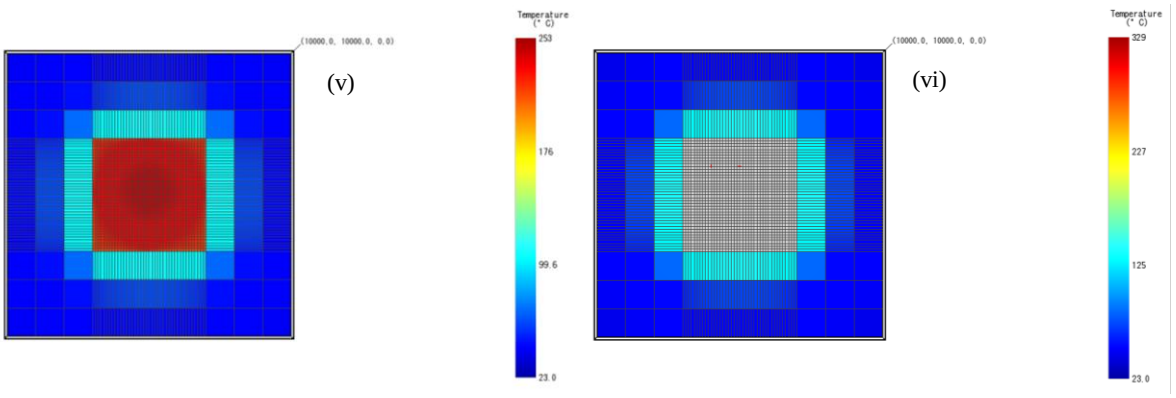

Appendix C

Temperature map for fault hosted permeability model (i) Base Case, (ii) 800mD, (iii) 100mD, (iv) 50mD, (v) 1100kJ/kg, (vi) 1500kJ/kg

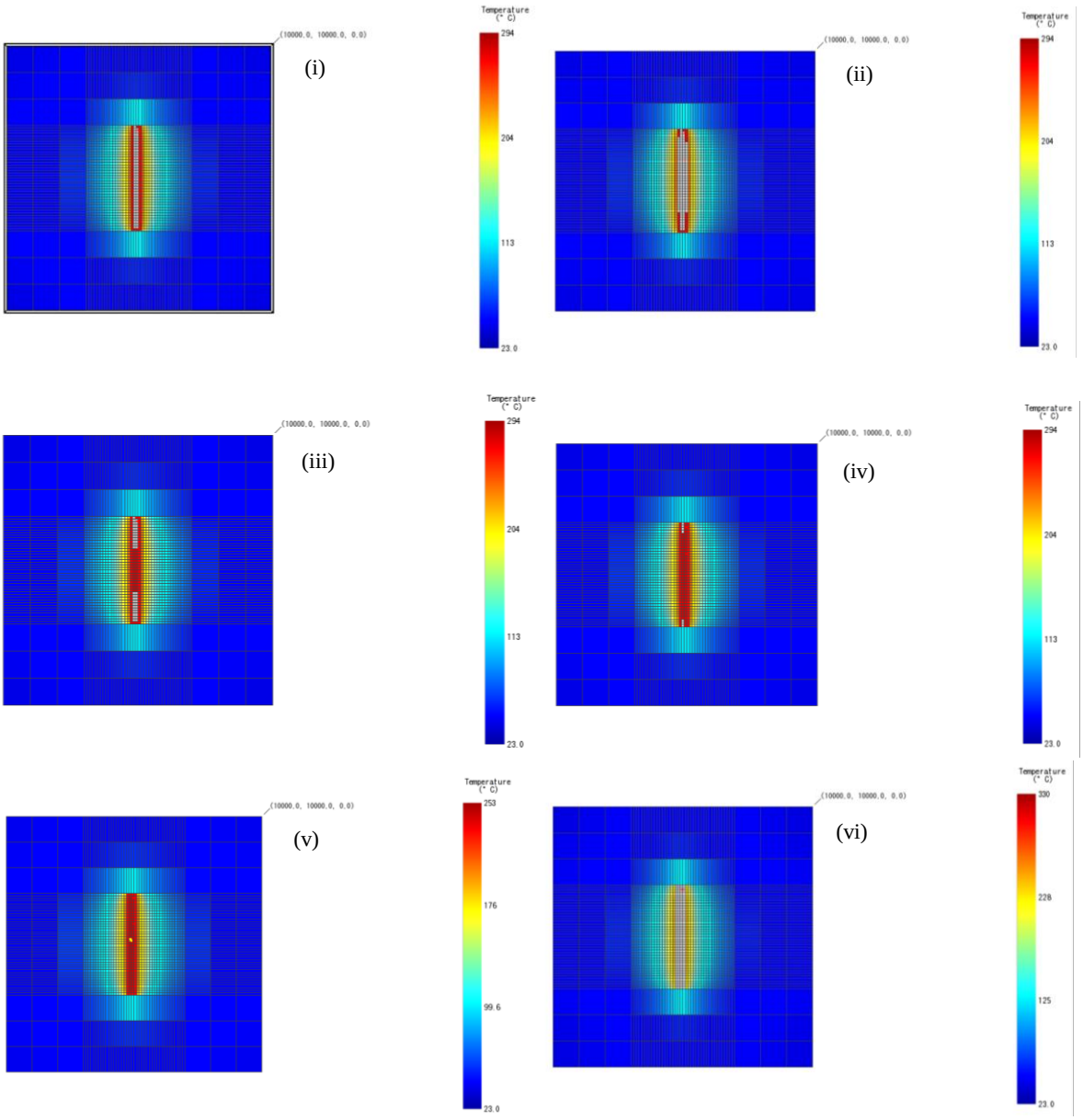

Appendix D

Thermal gradient map for distributed fracture model (i) Base Case, (ii) 800mD, (iii) 100mD, (iv) 50mD, (v) 1100kJ/kg, (vi) 1500kJ/kg

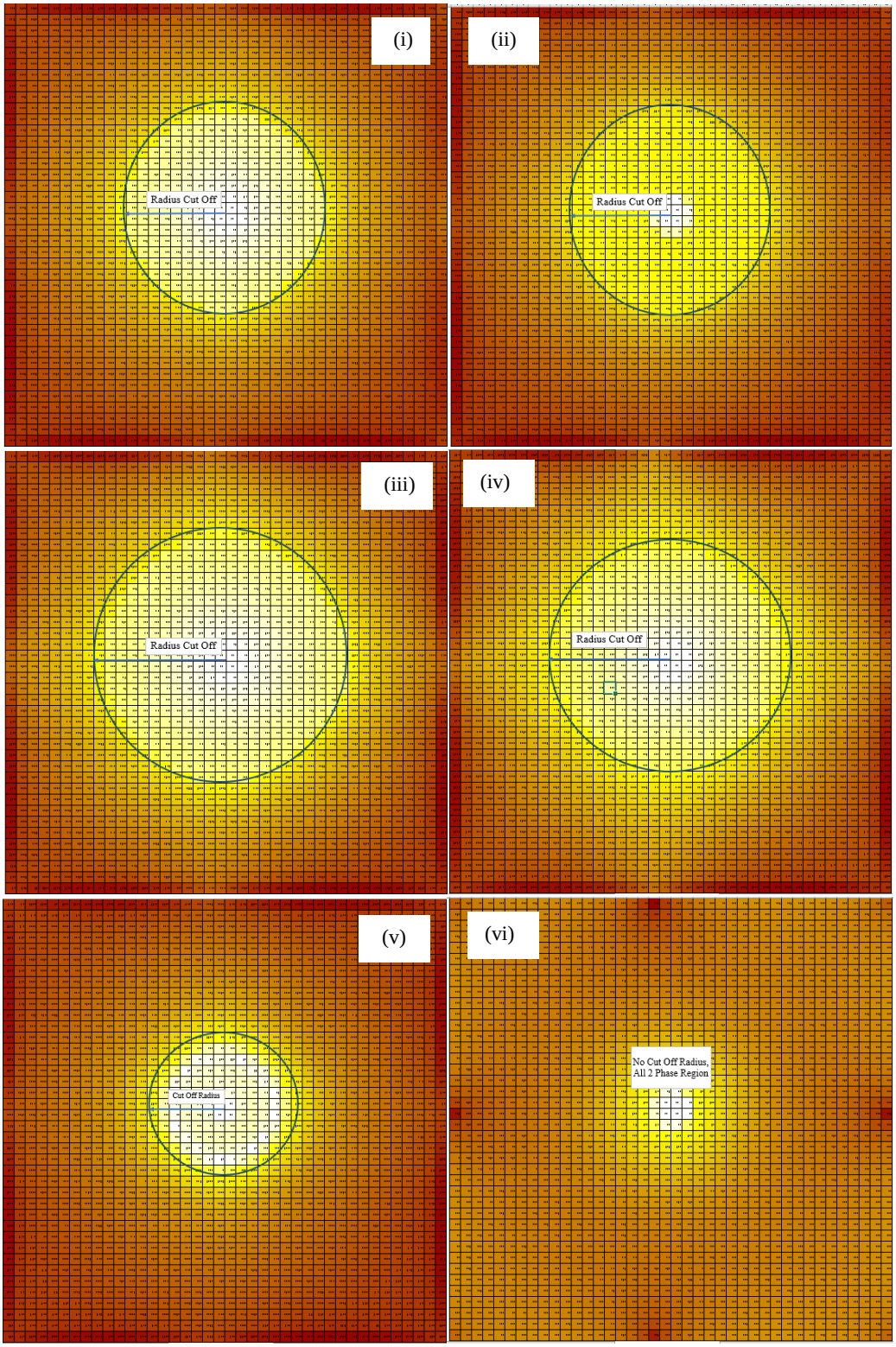

Appendix E

Thermal gradient map for fault hosted permeability model. (i) Base Case, (ii) 800mD, (iii) 100mD, (iv) 50mD, (v) 1100kJ/kg, (vi) 1500kJ/kg (left to right)